The Effect of Dye-Dye Interactions on the Spatial Resolution of Single-Molecule FRET Measurements in Nucleic Acids

Nicolas Di Fiori[†] and Amit Meller[†‡*]
[†]Department of Physics and [‡]Department of Biomedical Engineering, Boston University, Boston, Massachusetts

ABSTRACT We study the effect of dye-dye interactions in labeled double-stranded DNA molecules on the Förster resonance energy transfer (FRET) efficiency at the single-molecule level. An extensive analysis of internally labeled double-stranded DNA molecules in bulk and at the single-molecule level reveals that donor-acceptor absolute distances can be reliably extracted down to ~3-nm separation, provided that dye-dye quenching is accounted for. At these short separations, we find significant long-lived fluorescence fluctuations among discrete levels originating from the simultaneous and synchronous quenching of both dyes. By comparing four different donor-acceptor dye pairs (TMR-ATTO647N, Cy3-ATTO647N, TMR-Cy5, and Cy3-Cy5), we find that this phenomenon depends on the nature of the dye pair used, with the cyanine pair Cy3-Cy5 showing the least amount of fluctuations. The significance of these results is twofold: First, they illustrate that when dye-dye quenching is accounted for, single-molecule FRET can be used to accurately measure inter-dye distances, even at short separations. Second, these results are useful when deciding which dye pairs to use for nucleic acids analyses using FRET.

INTRODUCTION

The ability to probe biomolecular dynamics at the level of an individual complex has allowed scientists to explore biological processes with unprecedented detail. In contrast to bulk measurements, single-molecule experiments provide an opportunity to observe the detailed kinetics of individual biomolecules that might otherwise remain masked by ensemble averages (1,2). In particular, single-molecule Förster resonance energy transfer (sm-FRET) has become a popular technique due to its relative simplicity, high sensitivity, and ability to follow the dynamics of individual complexes over timescales relevant for many biomolecular processes (3,4). To date, sm-FRET has been broadly employed to probe the structure and dynamics of proteins and nucleic acids, DNA-protein interactions, RNA catalysis, and many other systems (5). However, most studies have been limited to the extraction of temporal information from transients and traces, although the evaluation of absolute donor-acceptor distances from sm-FRET data has remained controversial. A number of studies have found discrepancies at short inter-dye separations between the theoretically predicted and experimentally measured FRET efficiencies in the two most studied model systems used as molecular rulers, namely, polypeptides and double-stranded DNA (dsDNA) (6–10). It remains unclear whether these disagreements stem from a fundamental limitation in the method, or from shortcomings in the experimental systems employed (11,12). As a result, these inconsistencies restrict the spatial range and applicability of FRET as a spectroscopic ruler.

In this article, we analyze the effect of dye-dye interactions on the practical limits of sm-FRET using dsDNA molecules as a model system. We chose dsDNA for this study for its widespread use and relative simplicity with which high-purity DNA-dye conjugates can be synthesized. Moreover, this system benefits from the availability of a robust and simple structural model that predicts the inter-dye distances, allowing for a quantitative comparison of the FRET data with predicted distances (13). An extensive study of the dependence of FRET efficiency on inter-dye distances from ensemble and immobilized single-molecule measurements reveals outstanding agreement between these two and the model for donor-acceptor separations larger than ~5 nm. At shorter distances, however, a systematic inconsistency between the bulk FRET and the model prediction prompted us to closely examine the single-molecule traces. We find that at these distances donor-acceptor pairs exhibit correlated intensity fluctuations, which can be observed by either donor excitation through FRET, or by direct acceptor excitation. These fluctuations are characterized by well-defined intensity states, which alter the apparent measured FRET efficiency. When the efficiency is calculated using the intermittent photon intensity from the unquenched state, we obtain excellent agreement with the FRET efficiency values predicted by the dsDNA model, down to ~3 nm. As expected, the dye-dye interactions are dependent on the characteristics of the dye pair used. Here we examine four different donor-acceptor combinations; some display much stronger intensity fluctuations than others. We believe that these results are essential to understanding the basic mechanism underlying this phenomenon, which determines the photophysical properties of these and many other related systems.

Submitted October 5, 2009, and accepted for publication February 2, 2010.

*Correspondence: ameller@bu.edu

Editor: David P. Millar.

0006-3495/10/05/2265/8 $2.00

doi: 10.1016/j.bpj.2010.02.008

MATERIALS AND METHODS

Materials

A 57-basepair (bp) dsDNA (Integrated DNA Technologies, Coralville, IA) was used as a rigid scaffold to spatially separate the donor and acceptor FRET pair. A set of DNA constructs with different donor-acceptor distances were synthesized, with the acceptor fluorophore (*red*) always fixed and the donor position (*green*) varying, as shown in Fig. 1. The sequence of the strand containing the donor fluorophore was

$$5'\text{GCG GGC CGG GCG CGT TTT T}_{19}\text{T}_{18}\text{T}_{17}\text{T}_{16}\text{T}_{15}\text{T}_{14}\text{T}$$
$$\text{T}_{12}\text{TT}_{10}\text{TT}_{8}\text{T}_{7}\text{T}_{6}\text{T}_{5}\text{TT}_{3}\text{TT}_{1}\text{AT TTT TCG GGC GCG GCG}$$
$$\text{GGC} - 3',$$

with an amino-C6-dT residue (Integrated DNA Technologies) located at one of the subscripted thymines for conjugation with the dye. The complementary strand had the amino-C6-dT modification at its only thymine base. In this way, 14 constructs with distinct donor-acceptor separations (labeled D1A–D19A) could be generated. We used internal labeling to prevent end-stacking of nearly planar fluorophores, which has been shown to restrict their rotational freedom (14). Furthermore, as guanosine residues are well known to quench rhodamine dyes such as 5-carboxytetramethylrhodamine (TMR) through photoinduced electron transfer (15–18), we designed the region around the dyes to be a 29-bp-long poly(dA)-poly(dT) tract. This is structurally similar to B-DNA, except for a slightly smaller rise per bp (~3.1 Å), a wider major groove, and a narrower minor groove (19). G-C clamps were included at both ends of the molecule to keep the strands firmly annealed. All molecules included a biotin moiety attached to the 5′ end of the acceptor strand to facilitate immobilization to a streptavidin-coated surface.

Coupling reactions of the respective *n*-succinimidyl ester of the donor dyes, 5-carboxytetramethylrhodamine (TMR) (Invitrogen, Carlsbad, CA) and Cy3 (GE Healthcare, Little Chalfont, UK), and the acceptor dyes ATTO647N (abbreviated as A647N; ATTO-TEC, Siegen, Germany) and Cy5 (Invitrogen), were performed overnight in 0.1 M sodium tetraborate buffer (pH 8.5) at room temperature. Labeled oligonucleotides were then purified by 12% nondenaturing polyacrylamide-gel electrophoresis. Yield was ~50–70% and conjugation efficiency >95% as determined from absorption spectroscopy. Hybridization of the donor and acceptor strands were performed by mixing them in 1:1.25 ratio in 500 mM NaCl, heating the samples to 95°C, and then slowly cooling them down to 4°C over a period of 2.5 h.

Steady-state ensemble fluorescence spectroscopy

Bulk fluorescence measurements were carried out on a T-format spectrofluorometer (Jasco FP-6500; Jasco, Easton, MD) at room temperature using a 100-nM sample in buffer A (10 mM TRIS-Cl, pH 8.0 and 50 mM NaCl). Two emission spectra were collected for each construct: 1), when the donor dye was excited at 515 nm and emission was recorded from 535 to 800 nm; and 2), when the acceptor was directly excited at 615 nm with emission recorded from 635 to 800 nm (both measurements with 5:3 nm excitation/emission band-widths). As the extinction coefficients of the acceptor at 515 nm and of the donor at 615 nm are <2% of their maximum value, we neglected contributions from direct excitation of these dyes at those wavelengths. Donor leakage into the acceptor peak (~14%) was corrected by obtaining first a spectrum of singly-labeled dsDNA with donor only.

The fluorescence quantum yield of TMR attached to dsDNA in the poly(dA)-poly(dT) region was determined by comparison to a dilute fluorescent standard of known quantum yield, Rhodamine 101 (20), yielding $\Phi_{TMR} = 0.60$. The Förster radius R_0 for the TMR-A647N pair was obtained assuming substantial rotational freedom of the dyes ($\kappa^2 = 2/3$ approximation, see anisotropy measurements) and from the measured overlap integral of the spectra ($J = 7.8\text{E}{+}15\ \text{M}^{-1}\ \text{cm}^{-1}\ \text{nm}^4$), giving $R_0 = 67 \pm 4$ Å.

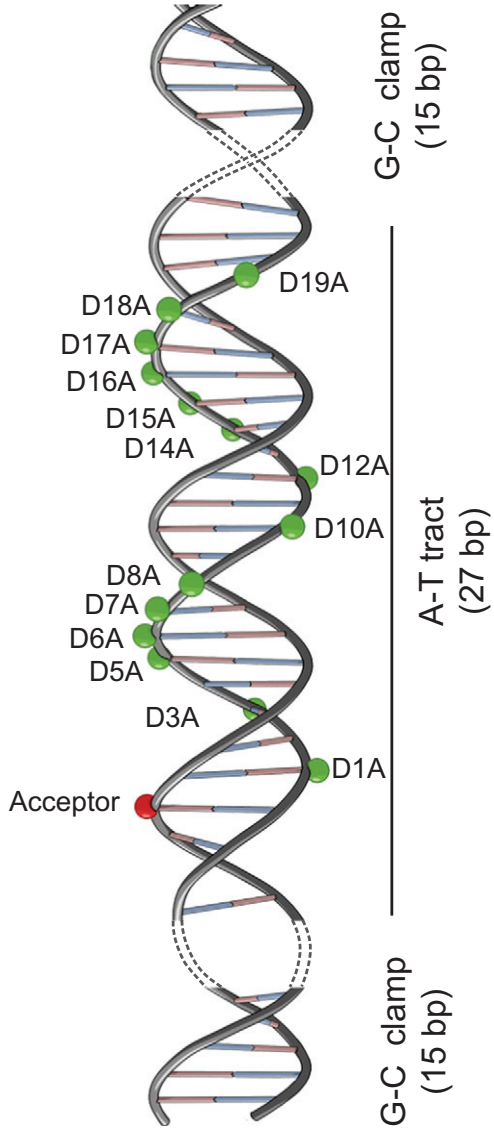

FIGURE 1 Schematic view of the dsDNA molecule showing the relative positions of the acceptor dye (*red*) and donor (*green*) as the latter was walked down the double helix. In this way, 14 constructs with varying donor-acceptor distances was generated, labeled D1A–D19A. The donor-acceptor pair was positioned on a homogeneous poly(dA)-poly(dT) tract that kept the nucleotide microenvironment, and hence Förster radius, identical for all inter-dye separations.

Steady-state and time-resolved fluorescence anisotropy measurements

Anisotropy measurements were performed on all constructs to verify that the changes in the measured FRET efficiencies were due to distance differences in the constructs, and not changes in the orientation of the dipoles. Measurements were performed using the steady-state spectrofluorometer and a FluoTime 100 (PicoQuant, Berlin, Germany) time-correlated single-photon counting instrument. Steady-state anisotropy values for TMR ($r_D = 0.12 \pm 0.01$) and A647N ($r_A = 0.19 \pm 0.01$) remained within the error range for all constructs D1A–D19A, and are significantly lower than the fundamental anisotropies. For all constructs, time-resolved anisotropy measurements found that the acceptor dye showed two mean rotational correlation times, $\rho_1 = 20 \pm 2$ ns (associated with DNA spin time) and $\rho_2 = 0.80 \pm 0.10$ ns

(associated with dye rotation). These values justify the approximation $\kappa^2 = 2/3$ used to obtain R_0 (10,21) and imply that the FRET efficiency for all constructs should be sensitive only to the inter-dye distance R.

Single-molecule fluorescence spectroscopy

Single-molecule traces were collected using an automated, dual-color (two excitation and two emission channels) confocal setup and a custom-built flow cell for sample immobilization as previously described (22). In short, a 514.5-nm line of Ar^+ laser (Spectra-Physics, Santa Clara, CA) and a 640-nm beam from a laser diode (iFlex 2000; Point Source, Hamble, UK) were expanded and attenuated to 5–15 μW and 3 μW, respectively, and directed into the back aperture of a 63×, 1.4 NA, oil immersion objective (Carl Zeiss, Oberkochen, Germany) mounted on a motorized x-y stage allowing coarse and fine motion using optically encoded DC motors and closed-loop piezo actuators, respectively (Physik Instrumente, Karlsruhe, Germany). The emitted light was filtered using a 514.5-nm notch (Kaiser Optics, Ann Arbor, MI) and focused on a 100-μm pinhole from where it was spectrally split using a 640 nm dichroic mirror (Chroma Technology, Bellows Falls, VT), and projected with 1:1 magnification onto two avalanche photodiodes (model No. AQR14; Perkin-Elmer, Wellesley, MA). Cross-talk was reduced using the appropriate filters, resulting in ~14% leakage of the donor emission into the acceptor channel and a negligible level of acceptor-to-donor leakage. The alternating laser excitation was performed at 50 Hz using an acousto-optic modulator and transistor-to-transistor logic modulation for the green and red lasers, respectively. The flow cell contained 30-μL chambers accessible by inlet and outlet fused silica capillaries connected to a buffer reservoir and a pump through flexible tubing. A custom control and data acquisition program written in LABVIEW (National Instruments, Austin, TX) was used to scan 20 × 20 μm^2 areas at 0.2-μm resolution, with a rate of 0.1 μm/ms. Data was processed to yield the intensity-weighted locations of all pixels above background counts. Molecules were then moved one at a time into the probing volume and the fluorescence of the donor and acceptor was recorded until the intensity of both dyes dropped to background levels. After all molecules had been probed, the stage was programmed to move to a new origin 100-μm away, and the scanning process was repeated. This allowed the unattended acquisition of hundreds of molecules overnight. An imaging buffer consisting of an enzymatic oxygen scavenger (glucose oxidase + catalase) and a triplet-state quencher (Trolox, >2 mM) was used to improve the lifetime and photostability of the fluorophores (23). Argon gas was bubbled into the buffer reservoir to prevent atmospheric oxygen from redissolving. The buffer was flown through the chamber at a constant rate and kept at a constant temperature of 22°C and pH level of 8.5.

Extracting FRET efficiencies from single-molecule traces

Our apparatus automatically records the donor and acceptor intensities from each molecule until both fluorophores photobleach, as observed by the abrupt reduction of the signals in both channels to the baseline level (24). Correction factors are needed to measure accurate FRET efficiencies and hence correct distances. To obtain these factors, we exclusively analyzed single-molecule traces in which the acceptor dye bleaches before the donor dye. These traces can be split into three separate regions: 1), while both dyes are active and energy is being transferred from donor to acceptor (region I); 2), after the acceptor has photobleached, but before the donor does (region II); and 3), after both dyes have photobleached (region III). From traces like these, we can extract the FRET efficiency for each individual FRET pair using

$$E = \frac{I_A}{I_A + \gamma I_D}, \quad (1)$$

where I_A and I_D are the background and cross-talk corrected acceptor and donor intensities in region I, and γ is a factor that accounts for the unequal quantum efficiencies of the dyes and of the two channels. Region II is needed to calculate this factor as well as to obtain the fraction of donor fluorescence leaking into the acceptor channel. Region III is used to correct the traces for background and to verify the presence of only one FRET pair in the probing volume. Because the acceptor absorption at the excitation wavelength is <2%, direct acceptor excitation is negligible. For each construct, at least 100 traces were individually analyzed to extract the single-pair γ-factor and transfer efficiency. The same procedure was applied to traces showing long-lived intensity fluctuations (see below).

RESULTS AND DISCUSSION

We first study the TMR-A647N donor-acceptor FRET pair due to their excellent quantum yield ($\Phi_{TMR} = 0.60$, $\Phi_{A647N} = 0.65$) and high photostability. Steady-state and time-resolved anisotropy measurements confirm nearly free rotation dynamics for all constructs (see Materials and Methods), justifying the approximation of $\kappa^2 = 2/3$. From bulk spectra measurement we find the Förster radius for this dye pair to be $R_0 = 67 \pm 4$ Å. In Fig. 2 we display typical single-molecule traces for six of the 14 different constructs with varying donor-acceptor separations. Moving from large (*top*) to small separations (*bottom*), we observe a clear trend: for separations larger than ~8 bp, donor and acceptor fluorescence intensities are steady over time, while at shorter inter-dye distances they show substantial fluctuations. These fluctuations are discrete and long-lived (hundreds of milliseconds to few seconds), alternating among two or three fixed levels. This is manifested in the all-point histograms from the acceptor intensities shown to the right of each trace (*red bars*). We can rule out several potential explanations for these fluctuations such as inter-dye distance variations or changes in dipole orientation, as those would have resulted in an anti-correlated donor-acceptor intensity behavior. Additionally, surface effects or fluorophore-DNA interactions alone cannot explain this behavior, because they would have affected all constructs alike, regardless of the donor-acceptor separation. Notably, this behavior is different from the long-lasting blinking observed in many red dyes (25) where the acceptor goes to a nonemitting state resulting in an anticorrelated increase of donor fluorescence.

A statistical analysis of 14 different dye-dye distances is presented in Fig. 3, where at least 100 traces were analyzed for each Δn value. On the left axis we plot the percentage of single-molecule traces displaying fluctuating intensity in the acceptor channel as a function of Δn (*solid circles*). We observe a clear transition from near-absence of fluctuating events for $\Delta n > 8$ to nearly 100% at the shorter donor-acceptor separations. Bulk measurements of the acceptor intensity, when excited through FRET (Ex = 515 nm), display a similar trend (*right axis*, *empty circles*): the fluorescence intensity of the acceptor dyes sharply decreases for $\Delta n > 8$, even though more energy is being transferred from the donor. The gradual reduction in acceptor intensity observed for $\Delta n > 12$ is expected due to the steady increase in donor-acceptor distance and hence weaker FRET

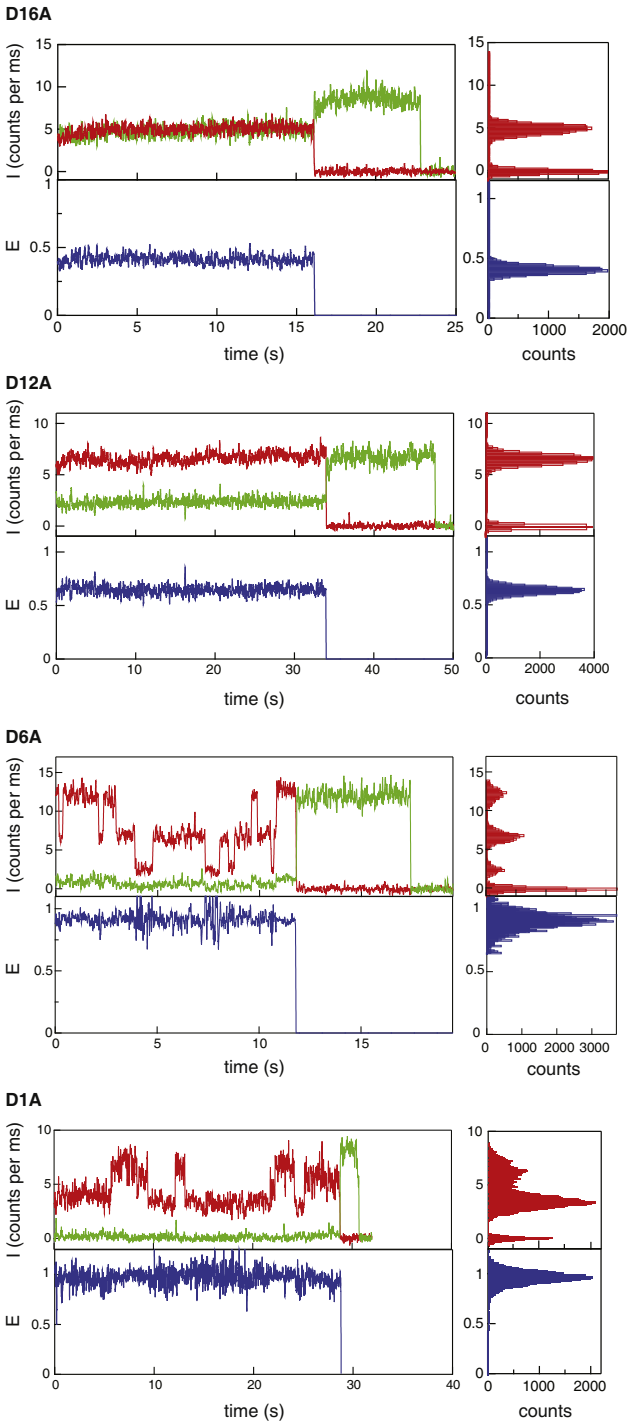

FIGURE 2 Representative single-molecule traces for donor-acceptor separations of 16, 12, 6, and 1 bp, with acceptor emission in red and donor in green. Below each trace, the FRET efficiency trace (calculated using Eq. 1) is shown in blue. The right panels show the all-point histograms for the acceptor intensity (*top*, *red*), together with the all-point histogram of the FRET efficiency (*bottom*, *blue*). As the FRET pair is moved closer together, the efficiency of the energy transfer increases, as expected. For short dye-dye separations ($\Delta n < 8$ bp), most traces show fluorescence fluctuating among two or three distinct intensity levels, as shown for samples D6A and D1A.

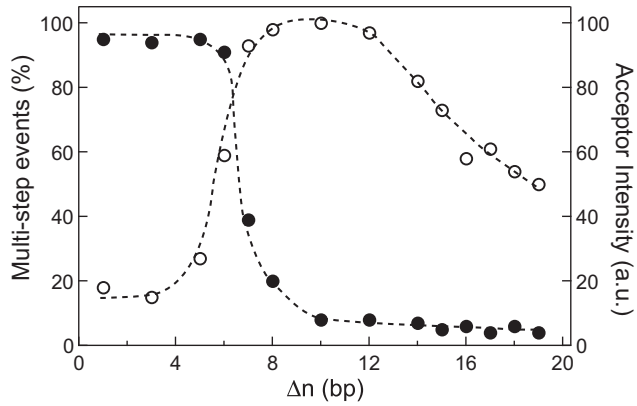

FIGURE 3 (*Left axis*, *solid circles*) Percentage of single-molecule traces showing intensity fluctuations in the acceptor channel. (*Right axis*, *open circles*) Acceptor fluorescence intensity from ensemble measurements when exciting the donor (Ex = 514 nm). $\Delta n = 8$ bp marks the transition from steady to fluctuating traces, which coincides with the separation at which a marked reduction in the acceptor emission in spectra is first observed. Dashed curves are guides to the eye.

efficiency. In all bulk measurements the concentration of the labeled DNA samples were kept constant to within 10% as verified by absorption spectra. We conclude that partial quenching of the acceptor dye, which is a prevailing phenomenon for short dye-dye distances, is, in part, responsible for the reduced bulk acceptor intensities. Fig. 3 and the single-molecule traces in Fig. 2 clearly indicate that donor and acceptor fluorophores interact with each other when they are positioned below 8 bp (~5 nm), and that this results in the formation of two new distinct long-lived quenched states.

Before we further characterize the intensity fluctuations observed at short separations, we consider the impact of the acceptor quenching on the measured FRET efficiency at the single-molecule level. The FRET efficiency E was calculated using Eq. 1, by evaluating the γ factor for each trace, as explained in Materials and Methods. The effect of the fluctuations on the transfer efficiency is seen in Fig. 2, where the trace of the FRET efficiency (*blue line*) is shown for each representative trace. For constructs with large separations, D16A and D12A, the E trace shows a single state. This is not the case for constructs showing fluctuations, D6A and D1A. The all-point histograms of E shown next to the traces reflect this trend, revealing much broader and asymmetric FRET distributions with wider tails toward lower values for the two constructs with shorter separations. A more extensive analysis showing this behavior is presented in Fig. 4. Here we calculated the distributions of the mean FRET efficiencies from hundreds of molecules from each construct. For traces showing more than one intensity level, the FRET efficiency corresponding to each level was individually measured. We show representative results for the four constructs discussed in Fig. 2. The two constructs with larger inter-dye distances show a distribution of transfer

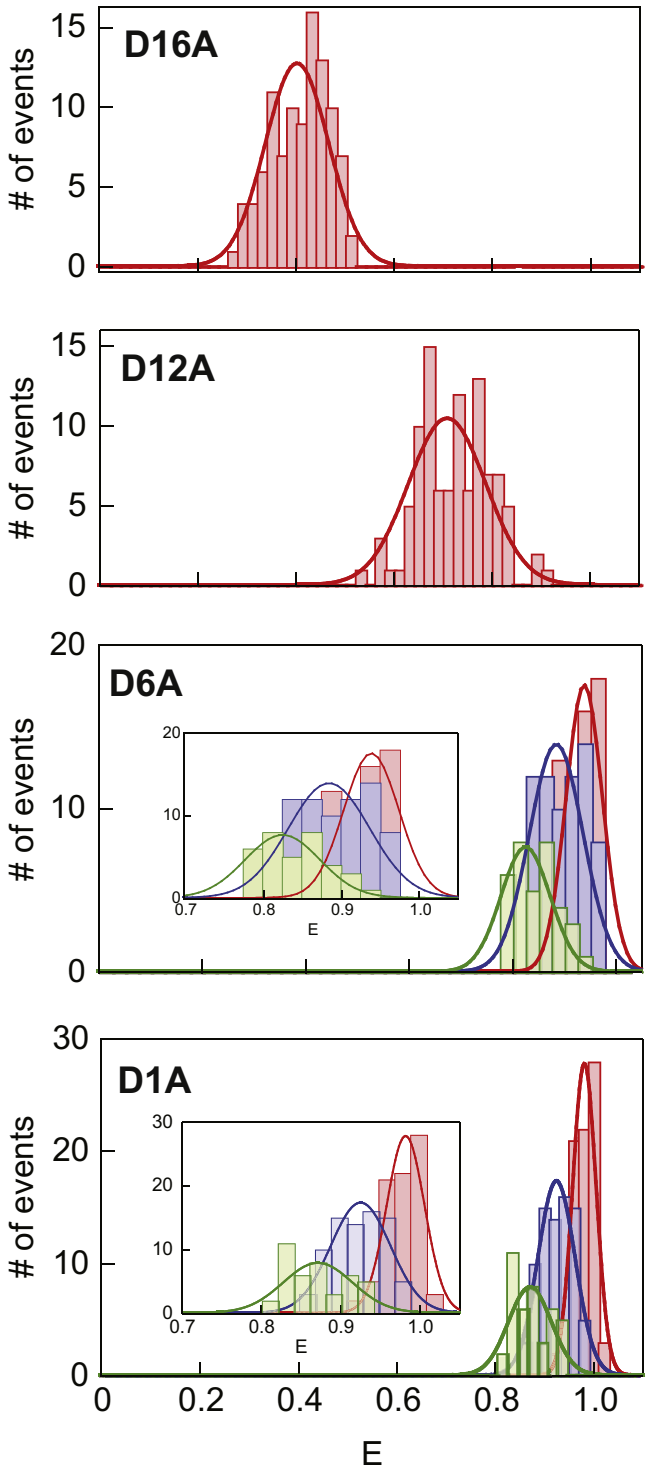

FIGURE 4 Histograms of average FRET efficiency from single-molecule traces for donor-acceptor separations of 16, 12, 6, and 1 bp. For the first two, the efficiencies can be well fitted using a single Gaussian distribution. In contrast, for the shortest separations, three Gaussians are needed, each corresponding to one intensity level (H, M, and L, see text) of the acceptor dye (*insets*).

efficiencies that can be fitted well using single Gaussian functions ($E_{\mathrm{D16A}} = 0.41 \pm 0.06$ and $E_{\mathrm{D12A}} = 0.72 \pm 0.04$, reduced χ-squares < 0.99). On the other hand, the distributions of transfer efficiencies for D6A and D1A show three distinct populations corresponding to the high (H), mid (M) and low (L) intensity levels, with different mean values ($E^{\mathrm{H}}_{\mathrm{D6A}} = 0.93 \pm 0.03$, $E^{\mathrm{M}}_{\mathrm{D6A}} = 0.90 \pm 0.04$, $E^{\mathrm{L}}_{\mathrm{D6A}} = 0.87 \pm 0.06$; and $E^{\mathrm{H}}_{\mathrm{D1A}} = 0.98 \pm 0.02$, $E^{\mathrm{M}}_{\mathrm{D1A}} = 0.93 \pm 0.03$, $E^{\mathrm{L}}_{\mathrm{D1A}} = 0.88 \pm 0.05$). These figures show that also, on a population level, the appearance of fluctuations in the acceptor at short distances systematically biases the measured FRET efficiency.

Fig. 5 displays the dependence of the measured FRET efficiencies on Δn for the 14 constructs with varying donor-acceptor separations, as obtained from single-molecule and bulk measurements. We use solid circles, solid squares, and solid triangles to differentiate the three FRET efficiency levels, H, M, and L, respectively, for $\Delta n > 8$. Our data is fitted using the geometrical model for dsDNA (13), where the donor-acceptor distance is approximated by

$$R_{\mathrm{mod}} = \sqrt{(3.1\Delta n + L)^2 + d^2 + a^2 - 2da\cos\theta}, \qquad (2)$$

and $\theta = 36\Delta n + \theta_0$. In Eq. 2, we use a 3.1 Å rise per base-pair, applicable for poly(dA)-poly(dT) trace, instead of the 3.4 Å appropriate for the B-form (19). The parameters d and a are the lateral distance of each dye from the helical axis (see *inset*), and L and θ_0 represent the components of the inter-dye distance parallel to the axis and the angle between the dyes in the lateral plane for $\Delta n = 0$, respectively. The solid line in Fig. 5 is a fit to the data using the Förster equation and Eq. 2 by means of the

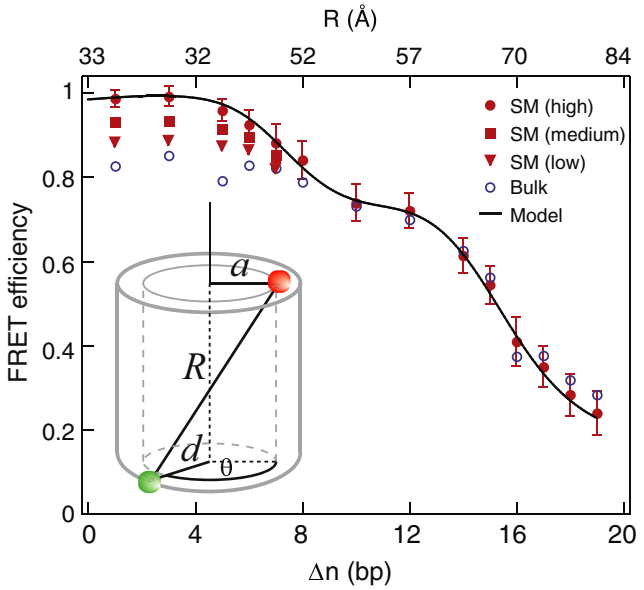

FIGURE 5 Single-molecule (*solid symbols*) and ensemble (*open circles*) FRET efficiencies as a function of donor-acceptor separation (in basepairs, *bottom axis*, and Ångstroms, *top axis*). (*Solid circles*, *squares*, and *triangles*) Values obtained from H, M, and L levels of the fluctuating traces (see text). (*Solid line*) Fit to the H level of the single-molecule data using the geometrical model for dsDNA (*inset*).

Levenberg-Marquardt nonlinear least-squares algorithm (IGOR Pro, WaveMetrics, OR), yielding an excellent agreement between the model and the sm-FRET data over the entire range of R values (shown at the top abscissa for reference), with the following values:

$$L = 16 \pm 4\,\text{Å}, d = 21 \pm 13\,\text{Å}, a = 9 \pm 6\,\text{Å},$$
$$\text{and } \theta_0 = 228 \pm 8^\circ.$$

The relatively large uncertainty obtained for the dye's linkers may suggest that the dyes dynamically change their relative position with respect to the DNA center with amplitudes of ~1 nm. This seems reasonable given the flexibility of the six-carbon linker connecting each dye to the corresponding base. In addition, the fit suggests that one of the dyes remains, on average, closer to the helical axis than the other, possibly due to stronger interactions with the nucleic acid. As A647N is a cationic and moderately lipophilic dye (26), we postulate that it binds to the major groove of the poly(dA)-poly(dT) tract, explaining the large value of L and smaller value of a. The somewhat higher steady-state anisotropy of the acceptor dye supports this interpretation (see Materials and Methods).

The excellent agreement between the model prediction and the single-molecule data is maintained only for the FRET values calculated at unquenched periods of the acceptor dye, E^{H}. The partially quenched states, E^{M} and E^{L}, yield values that are substantially lower than the prediction of the model. Likewise, the transfer efficiency values measured in bulk underestimate the efficiencies predicted by the model for small values of Δn (an additional possible source for the bias of bulk FRET when E is close to 1 is the inevitable presence of a small fraction of bleached acceptors). A similar trend has been observed in previous ensemble and single-molecule burst analysis measurements using TMR-Cy5, R6G-Cy5, TMR-JA133 (27), and ATTO520-Cy5 (28) for $\Delta n = 5$ bp, TMR-Alexa647 separated by 7 bp (10), and Alexa488-Cy5 separated by <9 bp (8).

The fluctuating intensity behavior observed from the single-molecule traces must have one of three possible characteristics: 1), the donor dye alone fluctuates among three distinct quenched states, or 2), the acceptor's quantum yield fluctuates among three values, or 3), both the donor and the acceptor dyes are simultaneously fluctuating among three quenched states. To discern which of these possibilities is responsible for the observed behavior, we performed single-molecule measurements using alternating laser excitation (ALEX) (10,25) through which the donor and acceptor dyes are alternately excited directly using 514-nm and 640-nm lasers, respectively. Fig. 6 (*top panel*) shows the fluorescence of the donor and acceptor when the 514-nm laser excited only the donor dye, and the bottom panel shows the donor and acceptor intensities when the acceptor dye was directly excited by the 640-nm laser. There is a perfect correspondence in the fluctuations of the acceptor,

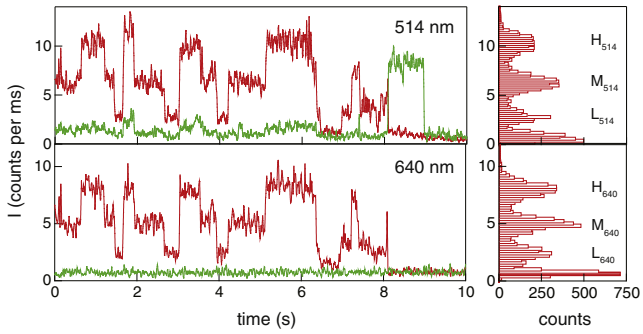

FIGURE 6 The sm-ALEX traces of construct D6A showing the donor (*green*) and acceptor (*red*) fluorescence when exciting the donor (Ex = 514 nm, *top panel*) and acceptor dye (Ex = 640 nm, *bottom panel*). The all-point histograms of the acceptor intensity reveal that the quenching levels, H, M, and L, are independent of the excitation mechanism. ALEX measurements prove that both donor and acceptor dyes are quenched simultaneously (see text).

regardless of whether it is excited directly or through FRET. Furthermore, the level of acceptor quenching—measured as the ratio of the intensity of the quenched states to the unquenched state—are identical, within our experimental accuracy ($M_{514} = 0.60 \pm 0.05$ vs. $M_{640} = 0.61 \pm 0.06$ and $L_{514} = 0.27 \pm 0.06$ vs. $L_{640} = 0.30 \pm 0.06$, relative to the unquenched levels H_{514} and H_{640}, respectively). Thus, the acceptor must be fluctuating among these three distinct states independently of FRET. Additionally, a closer inspection of the FRET trace (*top panel* and *traces* on Fig. 2) reveals fluctuations in the donor channel that are correlated to the ones in the acceptor channel, thus implying that the donor must also be fluctuating. Taken together, these observations imply that the interaction between the dyes result in simultaneous and synchronous quenching of both fluorophores.

Finally, we studied whether these long-lasting intensity fluctuations are specific to the TMR-A647N FRET pair. To do so, we replaced the donor with the cyanine dye Cy3 and the acceptor with Cy5, yielding three additional FRET pairs. In Fig. 7 *a*, we display representative single-molecule traces comparing these four different FRET pairs while keeping the donor-acceptor separation constant to 6 bp. From top to bottom, we display traces for Cy3-A647N, TMR-A647N, TMR-Cy5, and Cy3-Cy5. All-point histograms of acceptor intensity (*right-hand panels*) show three clear states for the two donors paired to the A647N acceptor, two states for TMR-Cy5, and a single acceptor state for Cy3-Cy5. The fraction of multistate acceptor levels (in a study comprising of >100 traces for each dye pair) is shown in Fig. 7 *b*. Although Cy3-A647N, TMR-A647N, and TMR-Cy5 show a significant amount of traces that display multiple acceptor intensity state, only the hydrophilic pair Cy3-Cy5 displayed <10% of fluctuating traces. Single-molecule alternating laser excitation (sm-ALEX) measurements for all FRET pairs show that, during fluctuations,

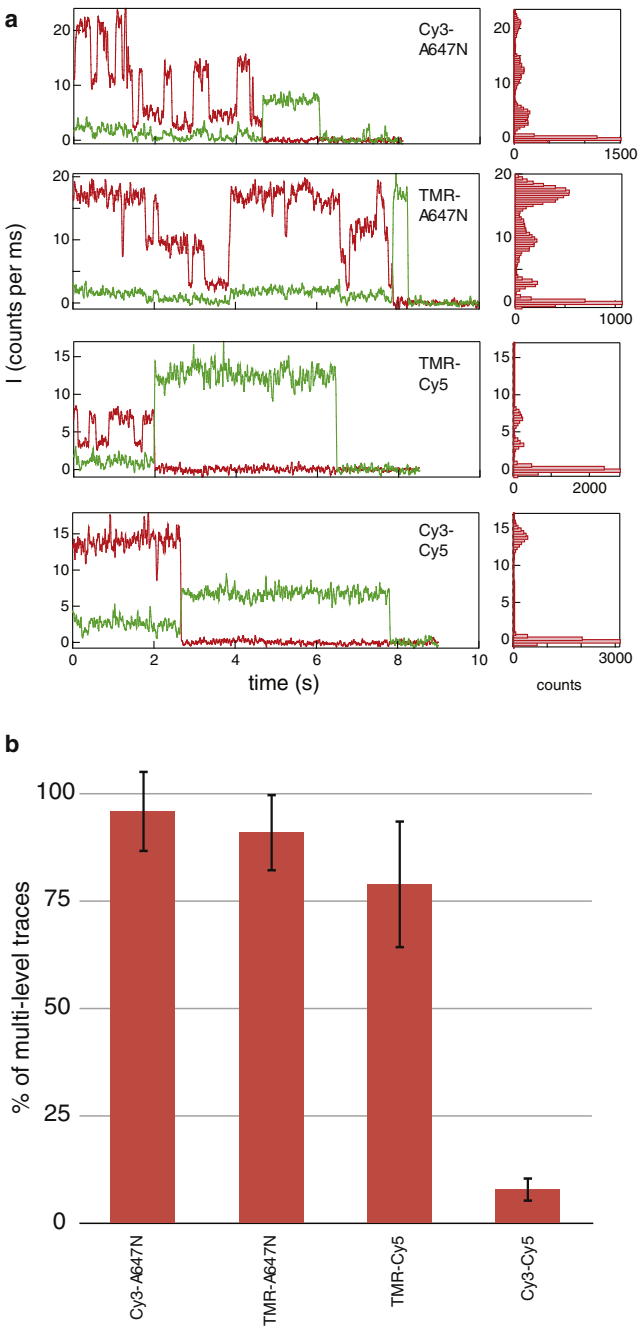

FIGURE 7 (*a*) Representative single-molecule traces and all-point histograms of acceptor intensity for Cy3-A647N, TMR-A647N, TMR-Cy5, and Cy3-Cy5 (*top* to *bottom*). In all cases the donor-acceptor distances was 6 bp. The acceptor dye A647N shows three well-defined states with distinct quenching efficiencies regardless of the donor with which it is paired. (*b*) Incidence of traces showing fluctuations in the acceptor intensity when the inter-dye distance is 6 bp for the four different FRET pairs.

both donor and acceptor dyes are quenched simultaneously as with TMR-A647N (data not shown). We point out that none of these constructs displayed fluctuating acceptor intensities for inter-dye separations of 10 bp, indicating that the origin of the effect is dye-dye interactions.

CONCLUSIONS

Using internally labeled double-stranded DNA molecules as rigid scaffolds, we have experimentally evaluated the range over which sm-FRET efficiencies can be used to faithfully report on the absolute donor-acceptor distances in this system. To avoid unwanted quenching of fluorophores by guanosine residues, we designed the labeling position to be a purely A-T tract. However, at short donor-acceptor separations (<5 nm), we observe long-lived fluorescence fluctuations from both dyes (TMR-A647N), which result in an apparent reduction of the average FRET efficiency when quenched and unquenched states are intermixed. We showed that when the FRET efficiency is evaluated from the unquenched portions of the single-molecule traces, we obtain an excellent agreement with a geometrical model over donor-acceptor distances from 3 to 8 nm. With the appropriate calibration, sm-FRET can be used to estimate intermittent donor-acceptor distance with high precision.

We established that the fluorescence fluctuations have their origin in dye-dye interactions, and are thus dependent on the FRET pair used. Even though Cy3-A647N and TMR-Cy5 show a significant number of fluctuating traces at short inter-dye distances, this phenomenon is largely reduced when the two cyanine dyes are paired together. The sm-ALEX measurements reveal that these interactions lead to the simultaneous and synchronous quenching of both dyes, regardless of the FRET pair used. The long timescales (hundreds of milliseconds to few seconds) of these quenched states may have excluded other spectroscopic techniques such as burst, fluorescence correlation spectroscopy, and photon-counting histogram from effectively characterizing this phenomenon. Furthermore, this fluctuating behavior might be misinterpreted as fictitious nucleic acid dynamics. On the other hand, immobilized single-molecule measurements allow the discrimination of the different quenching states throughout the entire lifetime of the fluorophores.

Absorption spectra show that direct fluorophore interactions, possibly resulting in the formation of hetero-dimers, occur at short distances (Δn = 1–5) but not for constructs with larger inter-dye separations, which still exhibit significant intensity fluctuations (see Supporting Material). This observation, together with other reports, suggests that an additional long-range mechanism such as DNA-mediated photoinduced electron transfer between the two fluorophores might explain the fluctuations observed at the single-molecule level (28–30). Although more-detailed studies are underway to reveal the underlying physical mechanism responsible for these midrange interactions, we are confident that these findings will be helpful when choosing the optimal FRET pair for nucleic acid studies.

SUPPORTING MATERIAL

One figure is available at http://www.biophysj.org/biophysj/supplemental/S0006-3495(10)00236-5.

We thank E. Atas, R. Clegg, M. Frank-Kamenetskii, E. Lipman, A. Squires, and J. Sutin for insightful comments on our manuscript.

A.M. acknowledges financial support from National Science Foundation award No. PHY-0646637.

REFERENCES

1. Weiss, S. 1999. Fluorescence spectroscopy of single biomolecules. *Science*. 283:1676–1683.
2. Selvin, P. R., and T. Ha. 2008. Single-Molecule Techniques. CSHL Press, Cold Spring Harbor, NY.
3. Forster, T. 1967. Mechanism of energy transfer. Chap. 2. *In* Comprehensive Biochemistry. M. Florkin and E. H. Stotz, editors. Elsevier, Amsterdam, The Netherlands.
4. Ha, T., T. H. Enderle, …, S. Weiss. 1996. Probing the interaction between two single molecules: fluorescence resonance energy transfer between a single donor and a single acceptor. *Proc. Natl. Acad. Sci. USA*. 93:6264–6268.
5. Selvin, P. R. 2000. The renaissance of fluorescence resonance energy transfer. *Nat. Struct. Biol*. 7:730–734.
6. Schuler, B., E. A. Lipman, …, W. A. Eaton. 2004. Polyproline and the ''spectroscopic ruler''' revisited with single-molecule fluorescence. *Proc. Natl. Acad. Sci. USA*. 102:2754–2759.
7. Deniz, A. A., M. Dahan, …, P. G. Schultz. 1999. Single-pair fluorescence resonance energy transfer on freely diffusing molecules: observation of Förster distance dependence and subpopulations. *Proc. Natl. Acad. Sci. USA*. 96:3670–3675.
8. Wózniak, A. K., G. F. Schröder, …, F. Oesterhelt. 2008. Single-molecule FRET measures bends and kinks in DNA. *Proc. Natl. Acad. Sci. USA*. 105:18337–18342.
9. Sahoo, H., D. Roccatano, …, W. M. Nau. 2007. A 10-Å spectroscopic ruler applied to short polyprolines. *J. Am. Chem. Soc*. 129:9762–9772.
10. Lee, N. K., A. N. Kapanidis, …, S. Weiss. 2005. Accurate FRET measurements within single diffusing biomolecules using alternating-laser excitation. *Biophys. J*. 88:2939–2953.
11. Camley, B. A., F. L. H. Brown, and E. A. Lipman. 2009. Förster transfer outside the weak-excitation limit. *J. Chem. Phys. JCPSA60021-9606* (in press).
12. Doose, S., H. Neuweiler, …, M. Sauer. 2007. Probing polyproline structure and dynamics by photoinduced electron transfer provides evidence for deviations from a regular polyproline type II helix. *Proc. Natl. Acad. Sci. USA*. 104:17400–17405.
13. Clegg, R. M., A. I. H. Murchie, …, D. M. Lilley. 1993. Observing the helical geometry of double-stranded DNA in solution by fluorescence resonance energy transfer. *Proc. Natl. Acad. Sci. USA*. 90:2994–2998.
14. Iqbal, A., S. Arslan, …, D. M. Lilley. 2008. Orientation dependence in fluorescent energy transfer between Cy3 and Cy5 terminally attached to double-stranded nucleic acids. *Proc. Natl. Acad. Sci. USA*. 105:11176–11181.
15. Torimura, M., S. Kurata, …, R. Kurane. 2001. Fluorescence-quenching phenomenon by photoinduced electron transfer between a fluorescent dye and a nucleotide base. *Anal. Sci*. 17:155–160.
16. Eggeling, C., J. R. Fries, …, C. A. Seidel. 1998. Monitoring conformational dynamics of a single molecule by selective fluorescence spectroscopy. *Proc. Natl. Acad. Sci. USA*. 95:1556–1561.
17. Seidel, C. A. M., A. Schulz, and M. H. M. Sauer. 1996. Nucleobase-specific quenching of fluorescent dyes. 1. Nucleobase one-electron redox potentials and their correlation with static and dynamic quenching efficiencies. *J. Phys. Chem*. 100:5541–5553.
18. Sauer, M., K. T. Han, …, K. H. Drexhage. 1995. New fluorescent dyes in the red region for biodiagnostics. *J. Fluoresc*. 5:247–261.
19. Nelson, H. C. M., J. T. Finch, …, A. Klug. 1987. The structure of an oligo(dA)·oligo(dT) tract and its biological implications. *Nature*. 330:221–226.
20. Vámosi, G., C. Gohlke, and R. M. Clegg. 1996. Fluorescence characteristics of 5-carboxytetramethylrhodamine linked covalently to the 5′ end of oligonucleotides: multiple conformers of single-stranded and double-stranded dye-DNA complexes. *Biophys. J*. 71:972–994.
21. Gohlke, C., A. I. H. Murchie, …, R. M. Clegg. 1994. Kinking of DNA and RNA helices by bulged nucleotides observed by fluorescence resonance energy transfer. *Proc. Natl. Acad. Sci. USA*. 91:11660–11664.
22. Sabanayagam, C. R., J. S. Eid, and A. Meller. 2003. High-throughput scanning confocal microscope for single molecule analysis. *Appl. Phys. Lett*. 84:1216–1218.
23. Rasnik, I., S. A. McKinney, and T. Ha. 2006. Nonblinking and long-lasting single-molecule fluorescence imaging. *Nat. Methods*. 3: 891–893.
24. Di Fiori, N., and A. Meller. 2009. Automated system for single molecule fluorescence measurements of surface-immobilized biomolecules. JoVE. http://www.jove.com/index/details.stp?id=1542.
25. Sabanayagam, C. R., J. S. Eid, and A. Meller. 2005. Long timescale blinking kinetics of cyanine fluorophores conjugated to DNA and its effect on Förster resonance energy transfer. *J. Chem. Phys*. 123:224708.
26. Eggeling, C., C. Ringemann, …, S. W. Hell. 2009. Direct observation of the nanoscale dynamics of membrane lipids in a living cell. *Nature*. 457:1159–1162.
27. Dietrich, A., V. Buschmann, …, M. Sauer. 2002. Fluorescence resonance energy transfer (FRET) and competing processes in donor-acceptor substituted DNA strands: a comparative study of ensemble and single-molecule data. *Rev. Mol. Biotechnol*. 82:211–231.
28. Kumbhakar, M., A. Kiel, …, D. P. Herten. 2009. Single-molecule fluorescence studies reveal long-range electron-transfer dynamics through double-stranded DNA. *ChemPhysChem*. 10:629–633.
29. Doose, S., H. Neuweiler, and M. Sauer. 2009. Fluorescence quenching by photoinduced electron transfer: a reporter for conformational dynamics of macromolecules. *ChemPhysChem*. 10:1389–1398.
30. Lewis, F. D., T. Wu, …, M. R. Wasielewski. 1997. Distance-dependent electron transfer in DNA hairpins. *Science*. 277:673–676.